Poly(amidoamine)-based Dendrimer/siRNA Complexation Studied by Computer Simulations: Effects of pH and Generation on Dendrimer Structure and siRNA Binding[a]

Kostas Karatasos,* Paola Posocco, Erik Laurini, Sabrina Pricl

In this work we report, compare and discuss the results obtained from fully atomistic molecular dynamics simulations of generations 4, 5, and 6 of PAMAM-based dendrimers having NH_3 and triethanolamine as cores, forming complexes with a short interfering RNA (siRNA) at different pH values and at physiological ionic strength. By employing a detailed analysis we demonstrate how features such as molecular size, structural details, and protonation level of this category of dendrimers affect the dendrimer/siRNA complexation. Properties like the conformational flexibility of the dendrimer, the effective charge distribution of the assembly, and the level of intra- and intermolecular hydrogen bonding between the two molecular entities are all found to play a significant role in the mutual interactions between the nucleic acid and the hyperbranched molecules. All these features are of key importance in the multifaceted mechanism of dendrimer/gene complexation, and their understanding can provide valuable insight toward the design of more efficient nucleic acid nanocarriers.

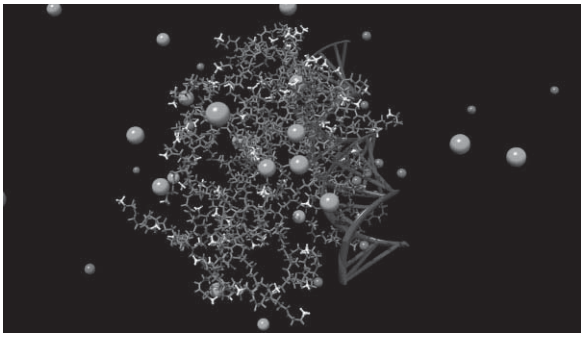

1. Introduction

The use of DNA or RNA for therapeutical purposes (gene therapy) is among the most promising routes for the effective treatment of several diseases, which in some cases are only poorly treatable by more conventional methods.[1] The principal challenge in gene-based therapeutic procedures is the assisted vehiculation and delivery of the nucleic acids (NAs) to the targeted sites. Other important issues are related, for instance, to the limited loading capacity of the carriers and to the control of related immunoresponse phenomena. In this respect, non-viral vectors have surged the activity of the scientific and industrial community

K. Karatasos
Chemical Engineering Department, Aristotle University of Thessaloniki, University Campus, 54124 Thessaloniki, Greece
E-mail: karatas@eng.auth.gr
K. Karatasos, P. Posocco, E. Laurini, S. Pricl
Molecular Simulation Engineering (MOSE) Laboratory, Department of Industrial Engineering and Information Technology (DI3), University of Trieste, Via Valerio 10, 34127 Trieste, Italy

[a] **Supporting Information** for this article is available from the Wiley Online Library or from the author.

DOI: 10.1002/mabi.201100276

toward the development of efficient and cost-effective NA delivery systems.[2,3] Synthetic carriers can be superior compared to viral vectors in terms of safety and flexibility of use.[2,4,5]

Hyperbranched polymers bear unique characteristics such as nanosized dimensions, multifunctionality, well-established chemistry protocols for modifying their functional groups (thus controlling their physicochemical behavior), as well as advantageous rheological properties which allow their efficient transfer to the targeted sites.[6,7] These features, when combined with low immunogenicity and biodegradability, render these molecules ideal candidates for the development of non-viral vectors for pharmaceutical and/or biological applications.[5,8–12] Understanding the essential mechanisms which govern the interactions involved in nucleic acid/dendrimer complexes (NADCs) which, to a large extent, affect the efficiency of these systems in gene delivery processes is therefore both a necessity and a challenge. To this ambitious goal, computer simulations have already been employed as a valuable tool for the exploration of the properties of such systems.[13–23] To our knowledge, however, several aspects of the mechanisms related to the non-covalent association/dissociation between a nanovector and its NA cargo, the role of specific topological details, and the influence of the thermodynamic environment in which they operate, remain largely unexplored. Accordingly, in this work we tried to address such issues by focusing on the supermolecular complexes formed by two families of poly(amidoamine)-based dendrimers and a double-stranded (ds) 19 base-pair (bp) RNA sequence by means of detailed atomistic molecular dynamics (MD) simulations.

This specific RNA strand has been selected as it represents a prototype of a short interfering RNA (siRNA) molecule. Indeed, post-transcriptional gene silencing by short RNA interference has recently emerged as a promising route toward a targeted inhibition of gene expression.[24–29] Moreover, siRNA/dendrimer complexes are currently being tested as potential systems for gene therapy applications.[5,12,30–32] Recent experiments, however, revealed that the delivery efficiency of these nanovectors can be improved by appropriate modification of the structural features of the dendritic carriers.[27,33,34] Furthermore, key features found to influence the formation, stability, loading capacity, transport capability, and toxicity levels of the NADCs involve, among others (i) the size of the dendritic molecule, (ii) the different physiological pH levels in which they operate, which may induce protonation of ionizable groups and, thus, affect the surface charge of the dendritic molecule, and (iii) the ionic strength of the solution, which is related to the level of screening of electrostatic interactions.[7,27,35–40] Previous computational studies of complexes comprised by diethylamine-core PAMAMs and other dendrimer families with siRNA sequences have examined effects of size and conformational variations in the binding efficiency,[13,19,41] and elucidated the role of counterions and the presence of more than one dendrimer molecules in certain static, dynamic, and energetic characteristics related to the complexation process.[14,20,21]

To obtain a deeper insight of the relative importance of the aforementioned parameters in siRNA/dendrimer complexation, we performed extensive atomistic MD simulations of three generations of PAMAM-based molecules characterized by two different topologies in complex with a 19 bp, ds siRNA sequence. The supermolecular assemblies were simulated at different pH levels in aqueous solutions and in the presence of a physiological value of the ionic strength (150 mM). Moreover, the binding energies of the dendrimer generations currently employed for siRNA delivery (i.e., G4–G6) with the NA fragment at the pH values most relevant to biomedical applications, were also calculated. The paper is then organized as follows. In the following section we provide the details of the molecular models and simulation procedures employed. Our results, obtained by MD simulations, are presented and discussed in the next section. Finally, in the last section we summarize, draw conclusions and point out some directions for future work.

2. Models and Simulation Details

The two families of PAMAM-based dendrimers considered in this work substantially differ in the topology of their cores. In the first series the branching pattern emanates directly from a NH_3 core, while the alternative series is characterized by the presence of a triethanolamine (TEA) central unit,[27,42] as illustrated in Figure 1.

In the structure having TEA as the dendrimer core, the branching units start at a distance of ten successive bonds away from the central amine, whereas the prototype NH_3-core PAMAM dendrimers branch out immediately at the central nitrogen of the NH_3 core. These TEA-core dendrimers have been previously reported for their efficient interaction with RNA molecules and their effective delivery of siRNA molecules.[27,42]

The entire study is focused on systems of generation 4, 5, and 6, as these are commonly used in pertinent biological experiments.[35,37,43,44] The detailed effect of the different degree of protonation of the primary/tertiary amine groups (i.e., different pH values), was studied by performing simulations of G4–G6 molecules of both series at five different pH levels. For the higher generation systems considered (G5 and G6), we focused on physiological (7.4) and moderately acidic (5.6) pH levels, taken as representative values of blood stream and cytoplasm, and of endosomal environment ensuing endocytosis of the complexes,[45] respectively (see Table 1). The protonation

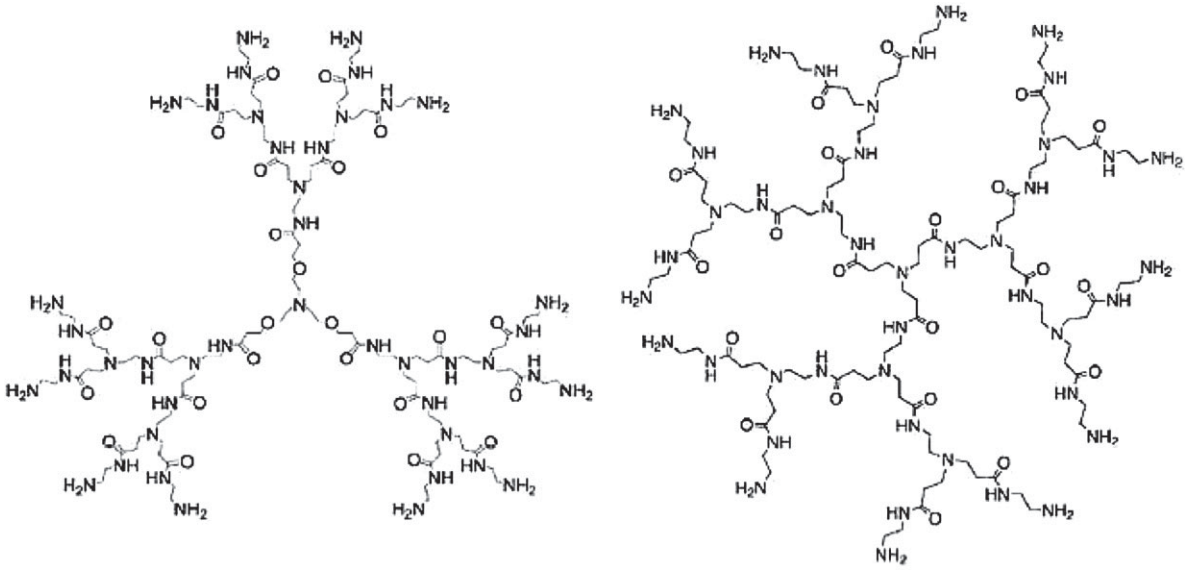

Figure 1. Chemical details of the TEA-core (left) and NH_3-core PAMAM dendrimers considered in this work. For clarity, dendrimers of the second generation (G2) are shown.

scheme adopted for both primary and tertiary amine groups in the NH_3- and TEA-based dendrimers (see Table 1) was based on an extensive campaign of DOSY NMR experiments performed on ethylene-diamine PAMAMs dendrimers at the same pH values considered in this work.[46] All dendrimer three-dimensional (3D) models were built following a well-consolidated procedure.[13,47–50]

The sequence of the 19 bp ds siRNA (i.e., CUUACGCUGAGUACUUCGA from the 3′ end to the 5′ end) was taken from our previous work.[13] In this paper, however, dendrimer and NA molecular models were parameterized using the CHARMM forcefield[51,52] (CHARMM22 for the dendrimers and CHARMM27 for the siRNA, respectively). This force field has been specifically optimized for the description of NAs models and their complexes,[53,54] and already successfully employed for modeling PAMAM dendrimers in combination with biological molecules.[55,56] To build the 3D models of the siRNA/dendrimer complexes, the siRNA strand was initially placed close to each dendrimer periphery using the VEGA ZZ software.[57] The resulting molecular pair was subsequently energy minimized to yield a starting structure devoid of substantial van der Waals overlaps. Each single dendrimer molecule as well as the corresponding siRNA complexes were then solvated with an appropriate number of pre-equilibrated TIP3P[58] water molecules extending at least 20 Å from the solute. A suitable number of Na^+ and Cl^- counterions were added to neutralize the system and to mimic an ionic strength level (based on free ions) of 150 mM[59] using the VMD software.[60] Eventual overlapping water molecules were removed.

Table 1. Number of the protonated primary/tertiary amines of TEA- and NH_3-core based PAMAM dendrimers used in the MD simulations at each pH value considered.

	pH				
G	4.0	5.6	7.4	8.4	12
4	48/46	48/31	44/1	22/0	0/0
5	96/94	96/64	87/3	45/0	0/0
6	192/190	192/129	168/6	90/0	0/0

Each molecular model was then subjected to a combination of steepest descent and conjugate gradient energy minimization steps (50 000 cycles), in order to relax close atomic distances. The energy-minimized systems were further equilibrated by performing 4–12 ns MD simulations in the isobaric-isothermal (NPT) ensemble using an integration step of 1 fs. During equilibration, different energetic components as well as static and conformational properties (e.g., radius of gyration of the dendrimer, average distance between the dendrimer and the siRNA molecules, and distribution of ions and water molecules around the complex) were monitored, to ensure their stabilization prior to production runs. MD production runs were performed on equilibrated systems again in the NPT ensemble with 1 fs time step ($T = 300$ K, $P = 1$ bar). The Langevin method for the control of temperature (with a damping coefficient of 5 ps^{-1}) and the Nose-Hoover Langevin piston method[61] for the control of pressure (using a piston period of 0.8 ps and a decay time of 0.4 ps) were employed for temperature and pressure control, respectively. Electrostatic interactions

were computed by means of the particle mesh Ewald (PME) algorithm.[62] Depending on the molecular dimensions of the examined systems, production MD trajectories of 4–6 ns were generated after the equilibration procedure, during which frames were saved every ps. The overall lengths of the trajectories thus produced were sufficient to achieve the complete decay of the global conformational relaxation of the dendritic component, as expressed by the autocorrelation function of the squared fluctuations of its radius of gyration (see Supporting Information).

As an example, Figure 2 depicts the initial configuration of the examined complexes after equilibration, at pH 7.4, as obtained following the aforementioned procedure.

To estimate the free energy of binding between each dendrimer and the siRNA molecule, we resorted to a well-established computational recipe[15,17,50,63] based on the so-called molecular mechanics/Poisson–Boltzmann surface area (MM/PBSA) methodology.[64] Accordingly, it will only be briefly described below (see Supporting Information for more details).

For a non-covalent association of two molecular entities $A + B \rightarrow AB$, the free energy of binding involved in the process may be generally written as $\Delta G_{bind} = G_{AB} - G_A - G_B$. For any species on the right hand side of this equation, from basic thermodynamics we have $G_i = H_i - TS_i$, where H_i and S_i are the enthalpy and entropy of the i-th species, respectively, and T is the absolute temperature. In view of this expression, ΔG_{bind} can then be written as: $\Delta G_{bind} = \Delta H_{bind} - T\Delta S_{bind}$. ΔH_{bind} is the variation in enthalpy upon association and, in the MM/PBSA framework of theory, can be calculated by summing the MM energies (ΔE_{MM}) and the solvation free energy (ΔG_{solv}), i.e., $\Delta H_{bind} = \Delta E_{MM} + \Delta G_{solv}$. ΔE_{MM} in turn is obtained from a single MD trajectory of the complex as $\Delta E_{MM} = \Delta E_{vdW} + \Delta E_{Coul}$, where ΔE_{vdW} is the variation of the nonbonded van der Waals energy and ΔE_{Coul} is the electrostatic contribution calculated from the Coulomb potential. The solvation term ΔG_{solv} is given by $\Delta G_{solv} = \Delta G_{ele} + \Delta G_{np}$, in which ΔG_{ele} is obtained by solving the Poisson–Boltzmann equation and ΔG_{np} is the nonpolar solvation term estimated via the semiempirical expression: $\Delta G_{np} = \gamma \times SASA + \beta$, in which SASA is the solvent accessible surface area of the molecule, γ is the surface tension parameter ($0.00542\ kcal \cdot Å^{-2} \cdot mol^{-1}$), and $\beta = 0.92\ kcal \cdot mol^{-1}$. Finally, the estimation of the entropic contribution $-T\Delta S_{bind}$ is performed using normal mode analysis, which requires the computation of eigenvectors and eigenvalues via the diagonalization of the Hessian matrix.

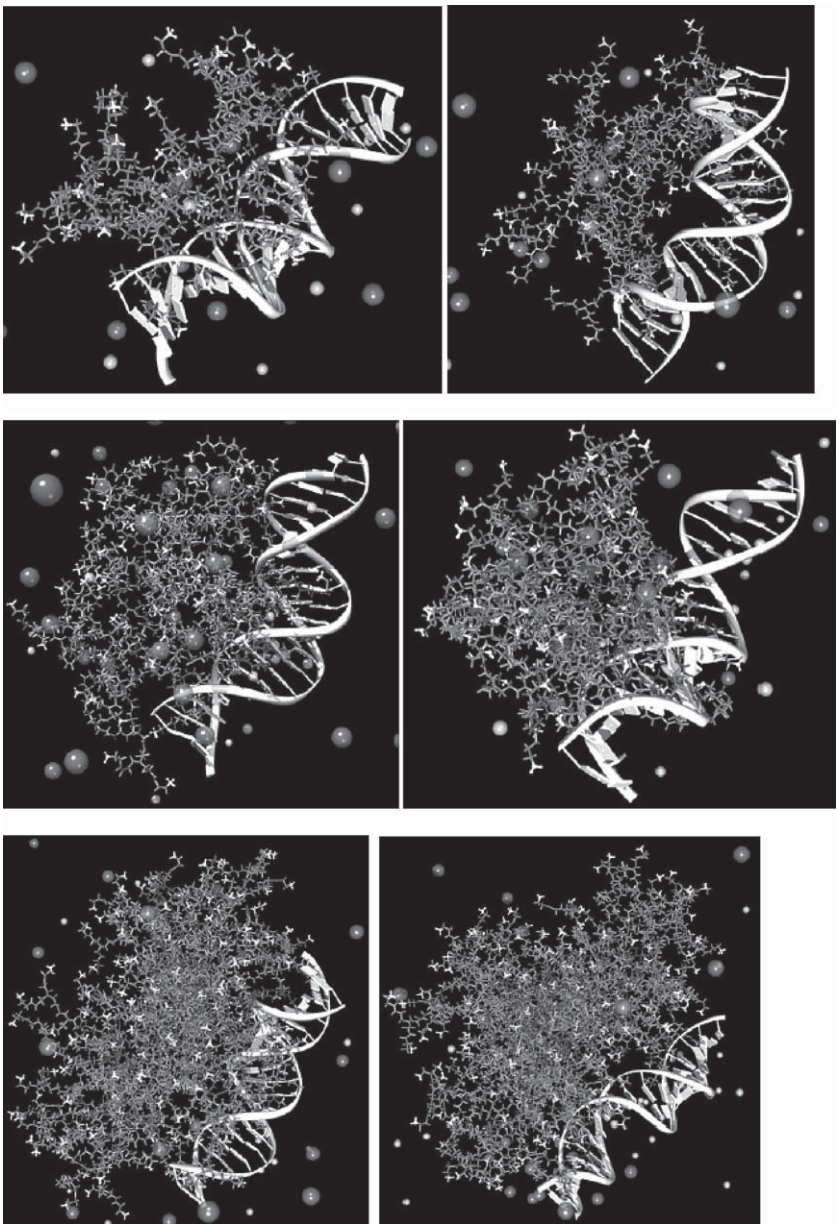

Figure 2. Equilibrated MD snapshots of the G4 (top panel), G5 (middle panel), and G6 (bottom panel) dendrimers in complex with siRNA at pH = 7.4. Left column, TEA-core PAMAMs; right column, NH_3-core PAMAMs. The dendrimer molecule is portrayed in mid gray sticks, with the terminal primary amine groups highlighted as light gray sticks-and-balls. The NA is depicted as a white ribbon. Cl^- and Na^+ are shown as dark gray and gray spheres, respectively. Water is not shown for clarity.

3. Results and Discussion

3.1. Static/Structural Study of the TEA- and NH_3-core PAMAMs in Complex with siRNA

As established by past experimental and simulation studies of NADCs involving PAMAMs as carriers, high generation (G4–G6) molecules are considered appropriate for gene delivery purposes while, due to their moderate size which allows them to behave as soft deformable particles rather than compact spheres, they offer a better control upon the response of their conformational properties to changes in the local environment.[5,41,44,65–67] This is unequivocally confirmed in the present study, as shown by the radius of gyration R_g curves in Figure 3(A) for G4–G6 of both dendrimer series in complex, with a 19 bp ds siRNA. Focusing on the TEA-core G4 molecule as a proof-of-concept, from Figure 3(A) we observe that there is a perceptible increase of the dendrimer average radius of gyration when the pH drops to values lower than 7.4, which amounts to ≈30% when considering the two extremes of the pH scale considered (i.e., 4 and 12). The same tendency of swelling with decreasing pH is exhibited by the higher generation dendrimers, as expected. It is worth noticing that for the most deformable systems of the 4th generation, the average dimensions appear smaller if compared to other experimental and simulation works of non-complexed G4 PAMAM dendrimers at similar pH values.[13,68] Interestingly, however, the TEA-core PAMAMs are more prone to swelling at lower pH values than their corresponding NH_3-based counterparts. This TEA-core dendrimer enhanced swelling capacity is intimately connected to the presence of an extended core, which endows these molecules with a greater structural flexibility and a more open conformation with void spaces in the interior. On the contrary, the NH_3-core series, with their three branches stemming directly from the small ammonia core, are more rigid and compact, with uniformly distributed monomer units and no restricted void spaces in the entire molecule.[69]

In harmony with these observations, the swelling of dendrimers upon protonation of the amine groups favors the penetration of a higher amount of water molecules within the TEA-core dendritic structure than in the NH_3-based structures, particularly at high generations and low pH conditions, as shown in Figure 3(B). Furthermore, the number of internal waters grows almost linearly with pH, paralleling the trend of R_g.

The systematic behavior exhibited by the G4 systems in the range of pH values considered is observed also for the higher generations (i.e., G5 and G6), albeit the degree of swelling is less pronounced than that observed for the smaller generations. This is not a surprising finding, since high generation PAMAM dendrimers are known to behave as rather compact particles.[13,19,68] Moreover, also for high generation numbers the molecules are characterized by the presence of an enlarged core, which reflects in an enhanced capacity of swelling for pH < 7.4 of TEA-core dendrimers with respect to the more rigid NH_3-core series. From a structure–activity standpoint, the enhanced swelling properties of TEA-core dendrimers at low pH values may lead to a higher buffering capacity which, in turn, can be beneficial to endosomal release of siRNA via the so-called proton sponge effect.[70] At the cellular level, in fact, inadequate cytosolic access in one major challenge that must be overcome if nanovector/siRNA systems are to become effective in vivo therapies. Thus, the supermolecular construct must efficiently mediate membrane translocation from the endosomal compartment into the cytosol, delivering its payload there, thus avoiding lysosomal degradation. The increased proton sponge effect of TEA-based dendrimers will allow these nanovectors to enter the endosome, adsorb protons, swell, and cause an influx of chlorine ions which, in turn, creates an osmotic effect

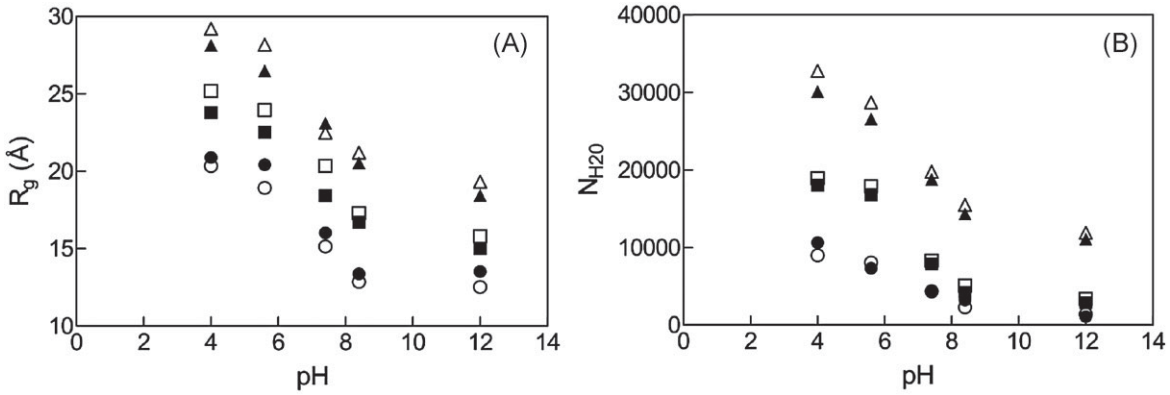

Figure 3. (A) pH dependence of the radius of gyration R_g, for G4–G6 TEA-core (open symbols) and NH_3-core (filled symbols) PAMAMs in complex with siRNA. (B) Number of water molecules within the G4–G6 TEA-core and NH_3-core PAMAM structures as a function of pH. Symbols as in panel (A). Symbol legend: circles, G4; squares, G5; triangles, G6. Error bars are smaller than symbols.

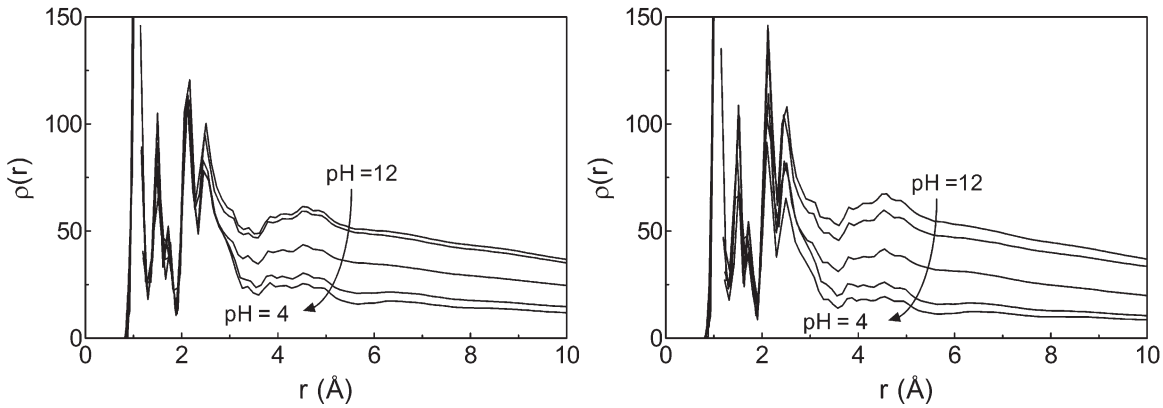

Figure 4. Radial distribution functions of TEA-core (left) and NH_3-core (right) G4 PAMAMs in complex with siRNA at different pH values. From top to bottom, pH = 12, 8.4, 7.4, 5.6, and 4.

leading to water influx. These events are purported to cause endosome membrane destabilization and rupture, with subsequent release of the nanovector/cargo complex in the cellular cytosol. The effective importance of the proton sponge effect is still somewhat debated. However, should this property play a major role in the overall transfection/silencing process mediated by PAMAM-based dendrimers, the present results concur to justify the enhanced transfection propertied of TEA-core based dendrimers with respect to the NH_3-core based counterparts under this perspective.

Generally speaking, changes in size upon protonation of their amine groups is known to induce significant intramolecular conformational changes in PAMAM dendrimers.[68,71,72] These, in turn, may affect their ability to form stable complexes with nucleotide sequences. Figure 4 shows the radial distribution functions $\rho(r)$ of the G4 systems taken as a proof-of-concept. Focusing on the peaks at distances around 5 Å, which refer to separations between atoms typically corresponding to structural units like dihedral angles, a systematic reduction of the peak amplitude is observed upon lowering pH. Such a loss of structural coherence with decreasing pH (as implied by the reduced probability of detecting distances corresponding to rigidity-related local structural units such as bending angles and torsions) is compatible with an enhancement of conformational flexibility of the dendrimers.

As can be inferred from this figure, a similar pattern characterizes the pH dependence of the radial distribution functions of the two dendrimer series. In fact, for both branched molecules an increase in their conformational flexibility is observed as their charge increases. As a consequence, their internal space widens, allowing more water molecules, counterions, and the NA fragment to penetrate inner parts of the dendritic architecture. A closer inspection of Figure 4 further reveals that three different "zones" of dendrimer conformational response to pH changes can be distinguished: a high pH zone (i.e., pH $\geq$ 8.4), an intermediate pH zone (pH = 7.4 here), and a low pH zone (i.e., pH $\leq$ 5.6). Indeed, the most prominent conformational variations are detected in the transitions

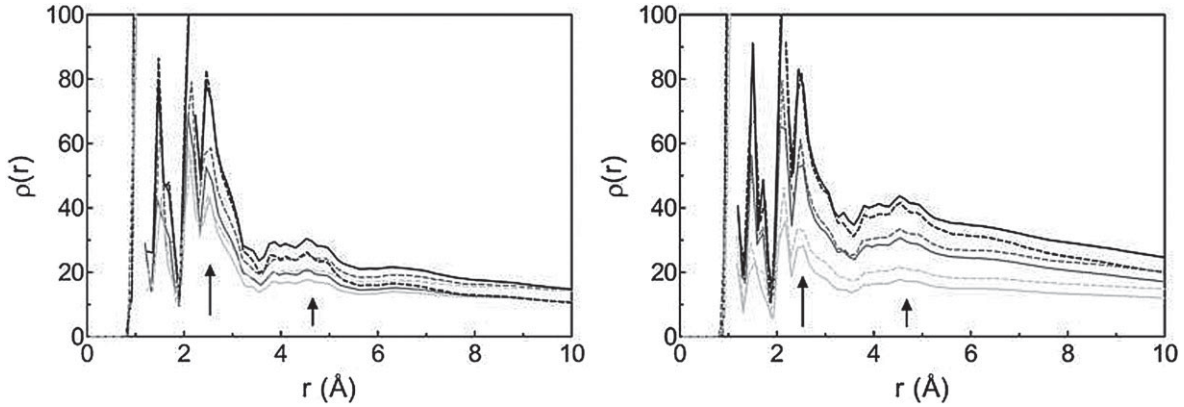

Figure 5. Radial distribution function of G4 (black), G5 (dark gray), and-G6 (light gray), TEA-core, and NH_3-core PAMAMs in complex with siRNA at pH 5.6 (left) and 7.4 (right). Continuous lines, TEA-core PAMAMS; broken lines, NH_3-core PAMAMs. Arrows indicate the distances at which changes in the amplitudes of the conformational peaks can be observed.

between the different zones, that is from pH = 8.4 to 7.4, and from pH = 7.4 to 5.6. The first conformational change (i.e., from high to intermediate pH) corresponds to the protonation of the majority of the primary amine groups, while the second conformational change (i.e., from intermediate to low pH) is detected when most of the tertiary, inner amine-groups bear a positive charge as well.

A different behavior, however, is seen for higher generation of both dendrimer series. In particular, at the two physiologically relevant pH values examined (7.4 and 5.6) only a weak reduction of the amplitude of the conformational peak in the range of 4–5 Å can be observed for the G5 systems, while no noticeable change is detected for the G6 molecules (data not shown). These indications allow us to conclude that, for the PAMAM-based dendrimers studied here, the variation of pH leads to small intradendrimer conformational rearrangements for high generation systems, in agreement with previous observations in other dendrimer families.[71,73]

For a better mapping of the dependence of the structural rearrangements on dendrimer size, in Figure 5 we compare the radial distribution function of the G4–G6 dendrimers at the two most physiologically important pH values.

As indicated by the arrows, the amplitudes of the peaks at distances associated with characteristic conformational units such as bending and torsional angles exhibit a systematic behavior upon variation of dendrimer generation, namely, the amplitude of the peaks decreases with increasing dendrimer size. However, this trend becomes less prominent as pH decreases. The loss of conformational coherence with increasing generation number suggests that at the same, constant protonation state, higher generation dendrimers retain a higher degree of structural flexibility at these local length scales.

To investigate how the conformational rearrangements triggered by changes in pH affect the complexation characteristics between a given dendrimer and its siRNA cargo, we monitored the density distribution of the siRNA molecule with respect to the center of mass of the dendrimer in the corresponding complexes, as shown in Figure 6.

As can be readily noticed, the siRNA profiles become broader and progressively shift toward the dendrimer interior as the pH level drops.

Interestingly, for the NH_3-core PAMAM G4, at both cellular-interesting pH values and, in particular, at pH 7.4, the siRNA seems to be able to penetrate somewhat deeper within the dendrimer interior than its TEA-core counterpart. At the lowest pH value no sensible differences can be discerned in the siRNA density profiles but, for the poorly protonated or the fully unprotonated states, a reverse situation can be envisaged, in which the siRNA is kept closer to the dendrimer surface in the case of the TEA-core PAMAM with respect to the NH_3-core case.

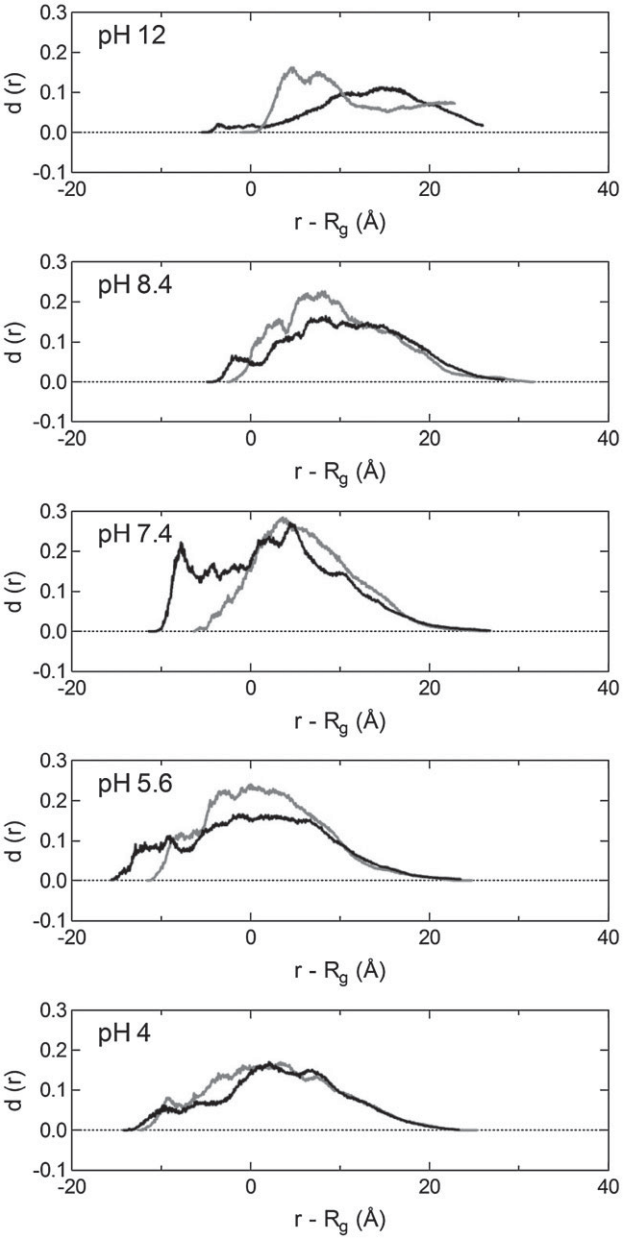

Figure 6. Density distributions of the siRNA strands with respect to the center of mass of the dendrimer in the corresponding complexes with TEA-core (gray) and NH_3-core (black) G4 dendrimers. Note that the distance r has been corrected for the dendrimer own radius of gyration (see text); accordingly, the o value on the *x*-axis indicates a distance corresponding to the radius of gyration of the dendrimer.

The main features of the distributions corresponding to the two examined dendrimer topologies share common characteristics. This is also reflected in the behavior of the average distance of the centers of mass between the siRNA cargo and its dendritic nanovector in each complex, as is illustrated in Figure 7.

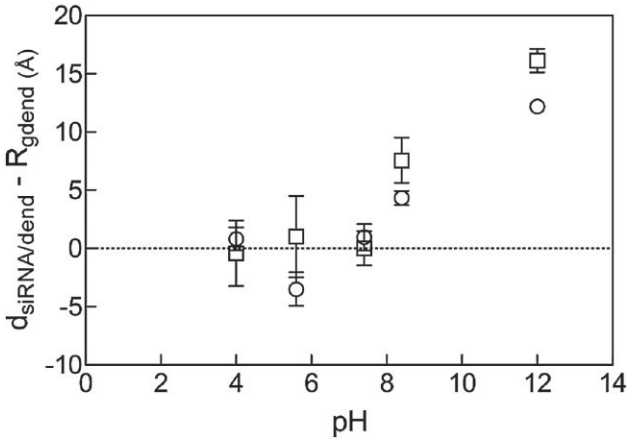

Figure 7. Average distance between the centers of mass of the G4 dendrimer and the siRNA, as a function of pH in the corresponding complexes. Symbols: TEA-core PAMAM, circles; NH_3-core PAMAM, squares.

From acidic to physiologically relevant pH levels (i.e., pH $\leq$ 7.4), the center of mass of the siRNA approaches that of the dendrimers at distances near to, or even closer than, the radius of gyration of the nanocarrier. In this respect, the protonation state being equal, the two systems bearing different cores behave in a similar manner within the error margins. Importantly, higher generation molecules follow an utterly analogous trend of these structural features as a function of the environmental pH. Although no conclusions regarding the association mechanisms between these two families of dendritic nanovectors and their siRNA payloads can be drawn at this stage, it appears that a threshold level of protonation does exist (i.e., 7.4) below which the average separation between the two molecular entities (i) is unaffected by the differences in dendritic topology and (ii) remains close to the dendrimer radius of gyration R_g.

3.2. Electrostatic Characteristics of the Dendrimer/siRNA Complexes

As proposed in several experimental studies focusing on the biophysical characterization of dendrimer/DNA complexes, electrostatic interactions play a significant role in the binding process of these molecules,[2,37,74] often sensibly ascribed to the interactions between the dendrimer positively charged amine groups and the negatively charged phosphate groups of the NA.[75] On the other hand, it has been demonstrated that, despite the structural similarity between siRNA and DNA with negatively charged anionic phosphodiester backbones, electrostatic interactions of siRNA with a cationic polymeric agent bear distinctly different characteristics.[29] On these accounts, and taking into consideration the implication of the electrical characteristics of the complexes in their biodistribution,[5] we tried to characterize the systems under study here in terms of their effective charge. In the effort toward obtaining a more accurate picture of these phenomena, we calculated the overall charge distributions of each dendrimer/siRNA complexes as a function of the distance from the center of mass of the dendritic molecule, taking into account the partial charges of all atoms belonging both to the dendrimer and the siRNA. Furthermore, in order to account for possible screening effects,[74] the charges of those counterions residing within the

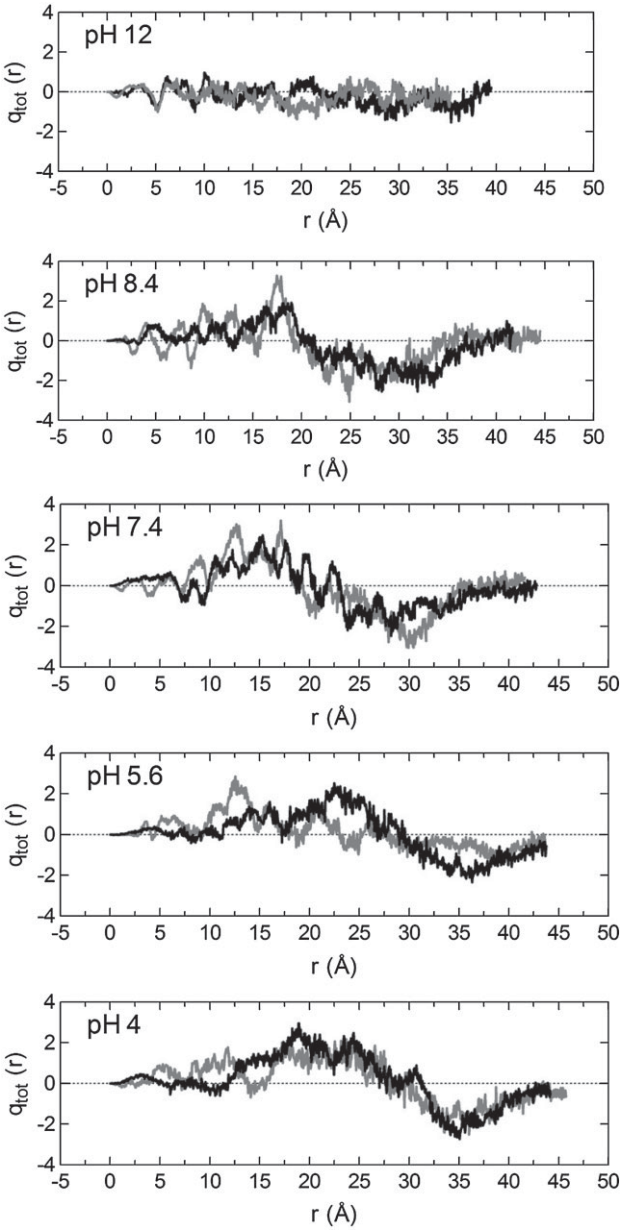

Figure 8. Effective charge distributions with respect to the center of mass of the dendrimer for the complexes of siRNA and TEA-core (gray) and NH_3-core (black) G4 PAMAMs at different pH values.

geometric boundaries of each molecular assembly were taken into account as well.

Figure 8 depicts the aforementioned effective charge distributions for the G4 systems at the different pH values examined.

Following the changes as the dendrimer protonation degree increases (i.e., shifting from a basic to an acidic environment), we observe the development of a charge modulation pattern. While close to the dendrimer center of mass the overall charge fluctuates around zero, an effective positive excess charge develops at intermediate distances which is followed by a negative effective charge at distances close to the dendrimer periphery. Within the statistical accuracy, this behavior characterizes all systems of both TEA- and NH_3-core series. The negative excess charge might be related to the presence of the negatively charged siRNA near the dendrimer surface. This notion is corroborated by the fact that the negative area of the profiles shifts toward longer distances from the dendrimer center of mass, in line with the expansion of the dendrimer dimensions upon increasing the dendrimer protonation state (see Figure 3). This finding indicates that, although the total effective charge of the complex remains close to zero (the negative section being approximately counterbalanced by the positive section of the curves), the complexes develop a sustained polar character. The emergence of the polar character of the complexes can already be observed at pH values close to physiological levels, implying that this mechanism may well affect the behavior of such complexes in in vitro and in vivo experiments conducted under physiological pH conditions.

Focusing attention on the pH values of physiological relevance, in Figure 9 we show the charge distribution curves for siRNA complexed by dendrimers of generation 5 and 6. Importantly, the main feature characterizing the charge behavior of the G4/siRNA complexes — that is the development of areas of excess positive and negative charge — is still present in these cases; however, significant

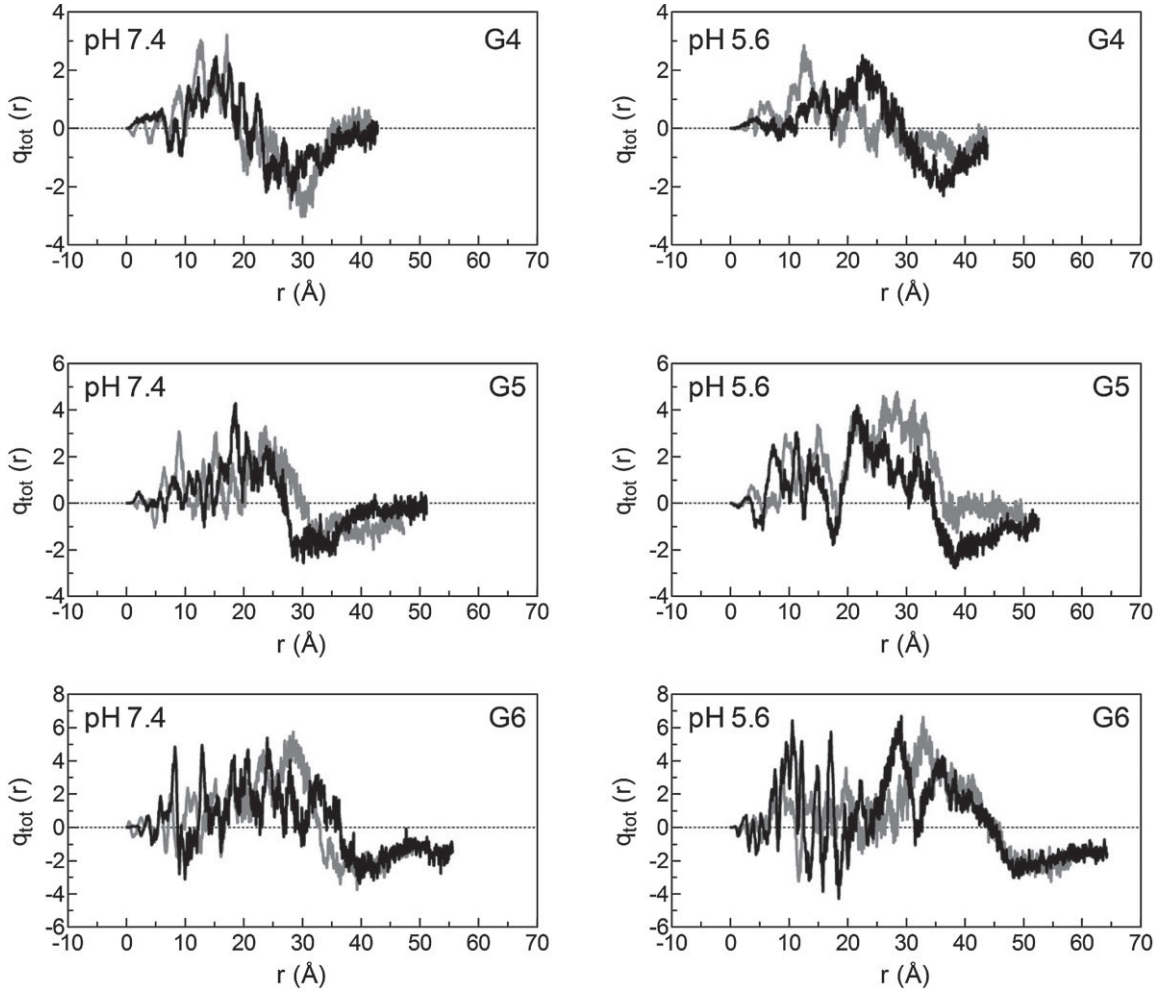

Figure 9. Effective charge distributions with respect to the center of mass of the dendrimer for the complexes of siRNA and TEA-core (gray) and NH_3-core (black) G5 and G6 PAMAMs at different pH values. To facilitate a direct visual comparison, the corresponding profiles of the G4 complexes shown in Figure 9 are included as well.

differences can also be noted. Aside from the fact that charge fluctuations within the dendritic structure seem to increase with increasing dendrimer generation, the electrically neutral part of the complex appears to extend at distances comparable to the radius of gyration of the dendrimer as generation grows.

In other words, for high dendrimer generation assemblies the polar area of the complex is mostly located close to the dendrimer surface rather than extending well within the dendrimer interior. This might be one of the aspects of the complex rationale underlying the enhanced siRNA binding and delivery capacity of these bigger nanovectors with respect to the smaller counterparts (vide infra).

3.3. Intra- and Intermolecular Hydrogen Bonding in the siRNA/Dendrimer Complexes

Previous experimental[76–80] and computational studies[50,68,81] have ascertained the important role played by hydrogen bonding in the formation of complexes between dendrimer as nanovectors and hydrogen-bond forming compounds (e.g., polymers, drugs, lipids, proteins, and NAs) as their cargos. Furthermore, this non-covalent interaction seems to contribute substantially during the process of cellular uptake by facilitating the interaction of the nanovector and the cell membrane.[30] In fact, hydrogen bonds have been deemed as (at least partly) responsible for the increased membrane penetration ability of internally charged PAMAM dendrimer/siRNA complexes.[30] Aside from the intermolecular hydrogen bonding between the components of a supermolecular complex or between the complex subunits and the solvent, because of their high degree of branching and the proximity of the branches imposed by the dendritic structure, dendrimer molecules are also well-known to form intramolecular hydrogen bonds. This last feature might actually affect the conformational properties of the dendrimer and, eventually, act antagonistically against the formation of hydrogen bond interactions between the dendrimer and the guest molecule(s).[68,81,82] To quantify the degree of intra- and intermolecular hydrogen bonding in the systems studied here, we focused our attention on characteristic atomic pairs which could potentially participate in such interactions in PAMAM dendrimers as well as in the NA fragment (siRNA).[75] Namely, to probe hydrogen bond formation within the dendritic structure we monitored the interactions between amine hydrogen (H) and carbonyl oxygen (O) pairs while, for the intermolecular dendrimer/siRNA hydrogen bonding, we analyzed the interactions between the dendrimer amine hydrogen (H) and the siRNA phosphate oxygen (OP) pairs.[5,83,84] Identification of a hydrogen bond was made based on commonly employed geometric criteria,[85–87] i.e., the distance d_{hb} between the relevant hydrogen and oxygen atoms lying within the proper range (typically close to 2–3 Å for the examined pairs) and the angle ϑ_{hb} between the N–H···O triplet was greater than 120° (see Supporting Information for more details on this point).

Figure 10 plots the average number of intramolecular H–O hydrogen bonds for the siRNA complexes based on the G4 dendrimers at different pH levels as an example. Apparently, both TEA-core and NH_3-core dendrimer series exhibit a similar non-monotonic behavior, the higher number of hydrogen bonds being achieved at the non-protonated state. The size of the vertical bars appearing in Figure 10 (and in the figures to follow as concerns hydrogen bonding information) reflects the fluctuation of the number of detected hydrogen bonds *per ps* (which corresponds to the frame-saving frequency of the MD trajectory) due to their rapid breaking and reformation which takes place at this timescale.[68]

As pH drops from highly basic conditions to physiological levels, the formation of intramolecular hydrogen bonds

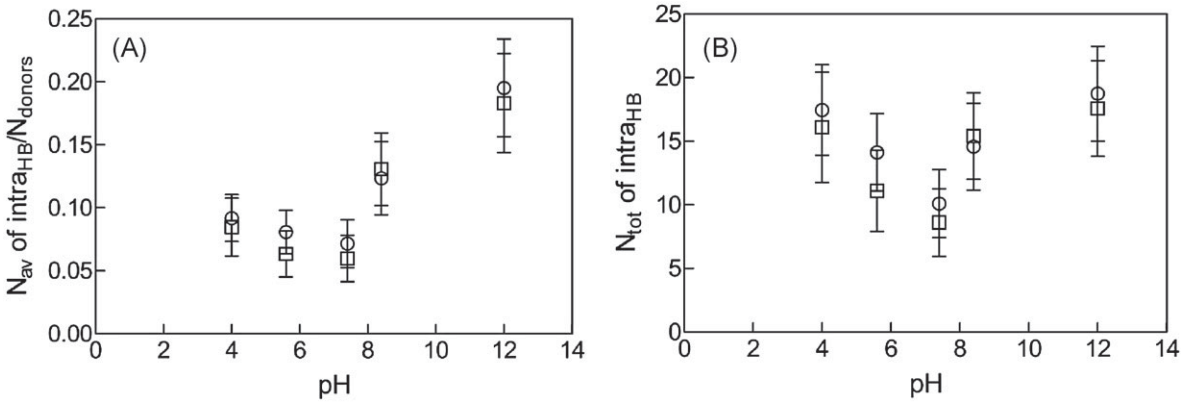

Figure 10. (A) Average number of the H–O intradendrimer hydrogen bonds per hydrogen donor and per timeframe, as a function of the pH for the G4/siRNA complexes. (B) Total number of intramolecular hydrogen bonds per timeframe in the same systems of panel (A). Symbols: circles, TEA-core PAMAMs; squares, NH_3-core PAMAMs. For the definition of the vertical bars see text.

depletes on average while for low pH values this trend seems to reverse. The initial suppression of intradendrimer hydrogen bonding upon protonation can be rationalized by taking into account the progressively increasing Coulombic repulsions among the positively charged amine groups, the consequent dendrimer conformational rearrangements to alleviate these repulsions, and the ultimate structure swelling. Indeed, such conformational adjustments result in a larger separation between the dendritic branches which, in turn, ultimately reflect in a reduction of the number of close contacts between potential donor/acceptor pairs. The subsequent tendency of an increasing number of hydrogen bonded pairs upon further protonation of the tertiary amines can be interpreted as a combined effect of different factors. On one hand, an increase of the protonation level leads to an increase of the number of hydrogen-bonding sites while, on the other hand, it generates a repulsion between the likely charged groups increasing thus the distance between the structural units they reside. In other words, the number of available donors can increase, but the number of hydrogen bonding events do not necessarily increase proportionally. There is, however, an additional factor that may influence the population of the detectable hydrogen bonds, and this is associated with the fact that hydrogen bonds involving charged groups tend to be energetically stronger[88] (see also Supporting Information). That is, even if the probability of the formation of hydrogen bonds might decrease by virtue of Coulombic repulsion, those bonds already formed can survive quite longer. The dependence of the dendrimer/siRNA intermolecular hydrogen bonds as defined above, is depicted in Figure 11 for the G4 systems.

As for the dendrimer intramolecular hydrogen bond case, the dependence of the intermolecular hydrogen bond formation between the nanocarrier and the NA fragment on pH follows a common pattern for both dendritic topologies examined within the estimated error levels. Generally speaking, the protonation of the amine groups for both systems facilitates the formation of dendrimer/siRNA H–OP hydrogen bonds (“H” and “OP” abide to the definition given earlier). Upon lowering pH, it appears that the larger increase in the population of H–OP hydrogen bonds takes place when passing from the state where the primary amines are partially protonated (i.e., pH = 8.4 in this work), to the state where almost all primary amines bear a positive charge (i.e., pH = 7.4 in this work). At least for the NH_3-core systems this increase lies beyond the error margins and the pH = 7.4 state appears to correspond to the protonation level which maximizes the population of the formed H–OP pairs. Notably, this maximum in the number of dendrimer/siRNA intermolecular hydrogen bonds seems to be correlated with the apparent minimum of the dendrimer intramolecular hydrogen-bonding pairs at the same pH value, as can be inferred by comparing Figure 11 and 10.

For complexes of higher dendrimer generations, the number of available hydrogen bonding sites increases with the number of the polar amine groups. The dependence of the extent of intermolecular H–OP hydrogen bonding on dendrimer generation at the most biologically interesting pH values of 7.4 and 5.6 is shown in Figure 12.

Focusing on the effect of dendritic topology, it appears that for the TEA-core systems at pH = 5.6 there is a systematic trend toward an increase in the examined hydrogen bonded pairs as generation grows. At the same pH level for the NH_3-core systems, only at the G6 complexes a substantial increase in the number of formed H–OP pairs can be observed. At pH = 7.4, no such systematic pattern can be distinguished, irrespectively of the dendritic topology.

Actually, when passing from G5 to G6 a trend for stabilization (TEA-core) or even a decrease (NH_3-core) of the number of hydrogen bonded pairs can be observed. These differences emphasize the role of the dendrimer generation and the protonation state in the efficacy of intermolecular

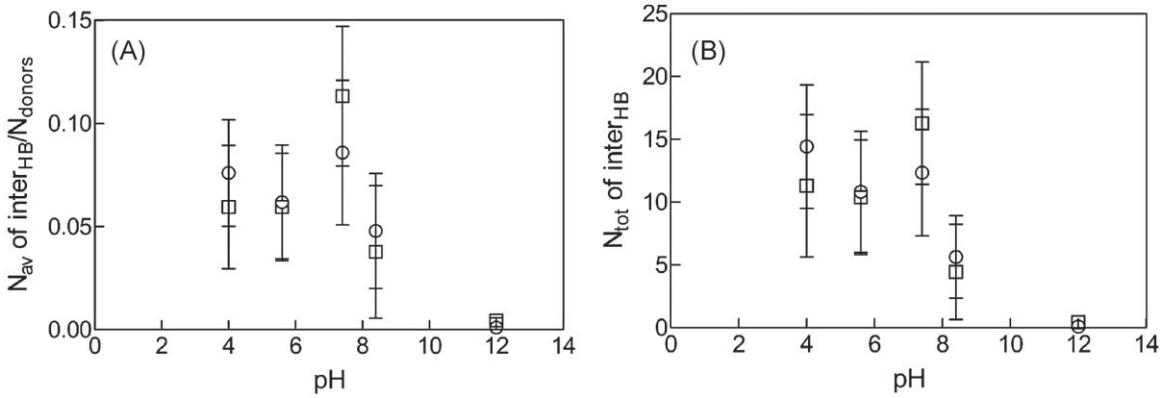

Figure 11. (A) Dendrimer—siRNA intermolecular hydrogen bonds per hydrogen donor and per timeframe, for the G4 PAMAMs as a function of pH (see text for the hydrogen bond pairs definition). (B) Total number of such intermolecular pairs per timeframe for the same systems of panel (A). Symbols: circles, TEA-core PAMAMs; squares, NH_3-core PAMAMs.

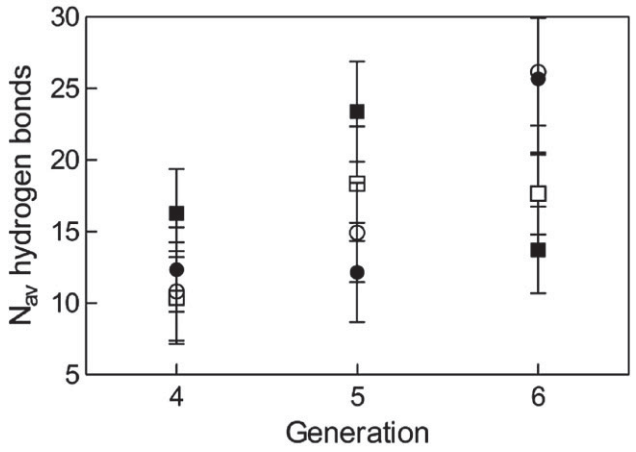

Figure 12. Number of intermolecular dendrimer/siRNA H–OP hydrogen bonded pairs per timeframe for all examined systems at pH = 5.6 (circles) and pH = 7.4 (squares). Open symbols, TEA-core PAMAMs; filled symbols, NH_3-core PAMAMs.

hydrogen bonding between the cargo and vector components of the complex. While for the G4 assemblies no significant differences could be noted between systems at both physiologically interesting pH states, for G5 nanoassemblies it seems that on average the number of H–OP hydrogen bonds peaks at pH = 7.4 whereas for the G6 counterparts this maximum localizes at pH = 5.6. These effects are most likely related to the different conformational characteristics of the G5 and the G6 dendrimers, where properties like the degree of backfolding or shape deformability — factors that might affect the relative location of the dendrimer amine groups — are known to be strongly dendrimer-size dependent.[65,89]

3.4. Free Energy of Binding between TEA- and NH_3-core Dendrimers and siRNA

To complement these structural investigations with some energetic considerations we performed MM/PBSA estimation of the free energy of binding ΔG_{bind} between G4–G6 dendrimers of both series and the chosen siRNA sequence at

Table 2. Analysis of the different energetic components involved in the dendrimer/siRNA binding in kcal · mol^{-1}.

			TEA-core PAMAMs pH = 7.4			
G	ΔH_{bind}	$-T\Delta S_{bind}$	ΔG_{bind}	$\Delta H_{bind}/N$	$-T\Delta S_{bind}/N$	$\Delta G_{bind}/N$
4	−432 ± 11	99 ± 10	−333 ± 15	−9.82	2.25	−7.57
5	−788 ± 13	133 ± 11	−655 ± 17	−17.9	3.02	−14.9
6	−902 ± 13	156 ± 10	−746 ± 16	−20.5	3.55	−17.0
			TEA-core PAMAMs pH = 5.6			
G	ΔH_{bind}	$-T\Delta S_{bind}$	ΔG_{bind}	$\Delta H_{bind}/N$	$-T\Delta S_{bind}/N$	$\Delta G_{bind}/N$
4	−507 ± 12	92 ± 9	−415 ± 15	−6.42	1.16	−5.25
5	−815 ± 11	133 ± 11	−682 ± 16	−10.3	1.68	−8.63
6	−1 299 ± 14	168 ± 10	−1 131 ± 17	−16.4	2.13	−14.3
			NH_3-core PAMAMs pH = 7.4			
G	ΔH_{bind}	$-T\Delta S_{bind}$	ΔG_{bind}	$\Delta H_{bind}/N$	$-T\Delta S_{bind}/N$	$\Delta G_{bind}/N$
4	−353 ± 16	152 ± 12	−201 ± 20	−8.02	3.45	−4.57
5	−702 ± 14	195 ± 10	−507 ± 17	−16.0	4.43	−11.5
6	−829 ± 13	210 ± 10	−619 ± 16	−18.8	4.77	−14.1
			NH_3-core PAMAMs pH = 5.6			
G	ΔH_{bind}	$-T\Delta S_{bind}$	ΔG_{bind}	$\Delta H_{bind}/N$	$-T\Delta S_{bind}/N$	$\Delta G_{bind}/N$
4	−398 ± 12	136 ± 9	−262 ± 15	−5.04	1.72	−3.32
5	−732 ± 12	158 ± 10	−574 ± 16	−9.27	2.00	−7.27
6	−1 136 ± 15	183 ± 12	−953 ± 19	−14.4	2.32	−12.1

the two most biologically significant pH values (5.6 and 7.4). In order to be able to compare the affinity of carriers of different generation toward the NA, the resulting values of ΔG_{bind} and its components (the enthalpy of binding ΔH_{bind} and the entropy variation upon binding $-T\Delta S_{bind}$) must be normalized by the total number of dendrimer charged amine groups N at a given pH. Accordingly, Table 2 lists both the actual and normalized values of ΔG_{bind} and its components for the whole set of complex systems.

As can be seen in Table 2, for all systems considered the free energy ΔG_{bind} is negative, which is favorable for binding. Moreover, the TEA-core PAMAMs show a superior affinity for the siRNA sequence with respect to their NH_3-core counterparts. As somewhat expected, the thermodynamic quantity governing the binding process in both cases is the enthalpy variation, which is also large and negative, and, hence, favors the binding between the siRNA and its vector. On the other hand, the entropy variations always afford an unfavorable contribution to binding. Actually, this is an expected result, as both molecules lose degrees of freedom upon complex formation with respect to their isolated states in solution.

Importantly, however, the behavior of the components of the binding free energy is not linear with dendrimer generation and pH, and shows both differences and similarities for the two PAMAM-like dendrimer families. In detail, we begin by noting that the enthalpy of binding ΔH_{bind} for both TEA-core and NH_3-core dendrimer/siRNA complexes increases almost linearly with increasing dendrimer generation at pH = 5.6, whilst it deviates from linearity for G5 at pH 7.4. Notably, this thermodynamic observation correlates directly with the observed trend in the number of intermolecular hydrogen bonds between the nanovectors and their cargos (see Figure 11). At the same time, the entropy contributions are seen to be lower (i.e., less unfavorable) in the case of TEA-core molecules, in particular at pH = 5.6. This lower value of $-T\Delta S_{bind}$ can be ascribed to a greater conformational change of the dendrimer (allowed by its high flexibility due to the large core) in order to enwrap the siRNA, followed by an enhanced productive bending of the NA for all generations in this dendrimer family. In other words, the conformation of the TEA-core dendrimers is such that the outer branches can readily move toward the phosphate backbone of DNA and the surface amino groups can arrange themselves via "induced-fit" for the optimal binding with DNA. This observation is somehow reminiscent of histones undergoing an induced fit conformational change when binding to DNA to form the nucleosome. A visual impression of the

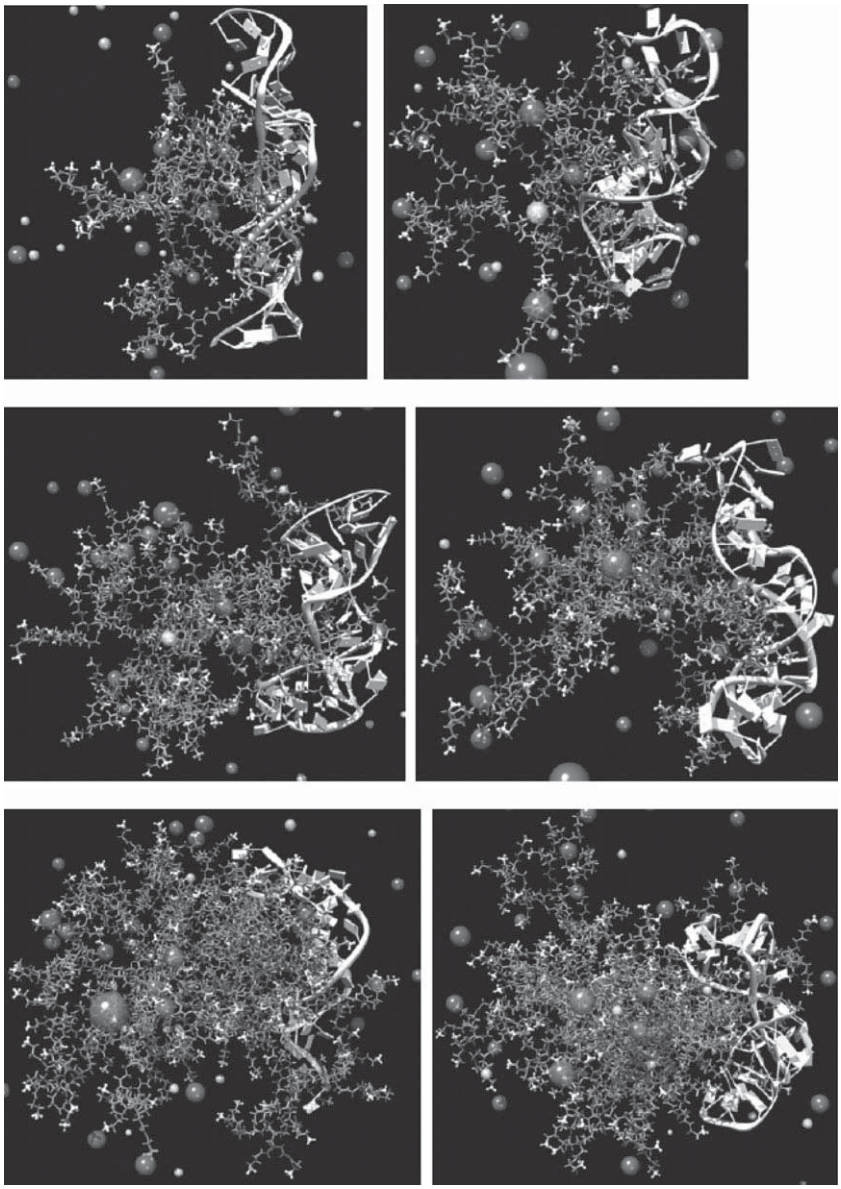

Figure 13. Snapshots from the MD production runs of the G4 (top panel), G5 (middle panel), and G6 (bottom panel) dendrimers in complex with siRNA at pH = 5.6. Left column, TEA-core PAMAMs; right column, NH_3-core PAMAMs. The dendrimer molecule is portrayed in mid gray sticks, with the terminal primary amine groups highlighted as light gray sticks-and-balls. The NA is depicted as a white ribbon. Cl^- and Na^+ are shown as dark gray and gray spheres, respectively. Water is not shown for clarity.

binding of the siRNA strands with the dendritic structure of the TEA-core and the NH_3-core dendrimers at the end of the production runs, is given in Figure 13.

Inspection of the snapshots implies that the "degree of integration" of the siRNA cargo into the dendritic structure is rather higher in the TEA-core systems (particularly in the larger generation models), in consensus with the analysis presented above.

4. Conclusion

Understanding the pathways and mechanisms governing the interactions of dendrimer/siRNA complexes and cells is crucial to making dendrimer-mediated gene delivery therapeutically viable. The complexity of the transfection process — from the nanovector/cargo assembly formation to its initial attachment to the plasma membrane, internalization of the complex via endocytosis, its release from the endosome followed by the dissociation of the vector from the siRNA followed by successful gene silencing — suggests that an interplay of many critically important parameters needs to be considered in order to achieve transfection. Optimizing all possible variables underlying this incredibly multifaceted pathway is a daunting task, if possible at all. Moreover, since nanovector-assisted delivery of NAs/small drugs is a multidisciplinary field by nature, any even small advancement in the knowledge of the chemistry, physics, biology, pharmacology, medicine, etc. of these systems is of paramount importance.

Under these perspectives, in this work we performed an extensive campaign of fully atomistic MD simulations on bimolecular complexes of PAMAM-based dendrimers and a 19 bp ds siRNA sequence, with the purpose of elucidating several structural/energetic aspects between the dendrimeric nanovectors and their siRNA cargo. All simulations were carried out in aqueous solutions under realistic conditions of ionic strength and different pH levels. Namely, in the study we considered effects of variations in the dendrimer branching topology (i.e., TEA-core and NH_3-core) and dendrimer size, on the static/structural characteristics, on the hydrogen bonding, and on energetic aspects describing the complexes.

Regarding the effects of the topological differences between the TEA-core and the NH_3-core systems *in the structural changes of the dendrimer hosts*, no drastic differences were observed especially at intermediate/low pH values for these macromolecules within the expected error. It appears, therefore, that in this pH range it is the nature and the number of the ionizable groups that concur to determine their behavior rather than the structural differences in their core region. However, in the intermolecular hydrogen bond network between the dendrimer and the siRNA in complexes of higher generation dendrimers, a certain differentiation in the average behavior can be unambiguously identified for the molecules of the two varying topologies. In addition, for all systems of both architectures, changes in the behavior of the complexes as a function of dendrimer size and pH are remarkable and systematic.

The effects associated with changes in pH (as probed mainly from the behavior of the G4 systems) are reflected by the conformational, electrostatic, and hydrogen-bonding characteristics of the formed complexes. Aside from the monotonic increase of the average dendrimer size with decreasing pH due to enhanced Coulombic repulsions, conformational rearrangements affecting the flexibility of the dendritic molecule take place upon gradual protonation of the amine groups as well. In fact, the lower the pH, the higher the observed degree of loss of dendrimer structural coherence at distances corresponding to local conformational units (i.e., bending and torsional angles). These changes appear to work synergistically with the development of a polar character of the complexes as pH levels decrease, in order to allow for a closer approach of the center of mass of the siRNA to that of the dendrimer, reaching separations even shorter than the R_g of the dendrimer. It is worthy to point out here the part that the counterions and the ionic strength play in this process, since their presence contributes decisively in the observed modulation of the effective charge. The development of a polar character in the complexes might actually create the driving force for the formation of supramolecular aggregates in non-stoichiometric dendrimer/NA systems.[21,37,74]

Variation of the pH level is also closely linked to changes in both the intramolecular and the intermolecular hydrogen bonding pattern in the complexes. It was found that, on average, close to physiological pH the number of intramolecular hydrogen bonding pairs within the dendrimer is minimized while, under the same conditions, the intermolecular dendrimer/siRNA hydrogen bond level reaches a maximum.

The effects of dendrimer generation at constant pH (at two physiologically relevant pH values of 5.6 and 7.4) become apparent through (i) the alteration of the dendrimer conformational characteristics such as the loss of structural flexibility upon increasing generation number, (ii) the "shift" of the polar region of the complex at distances closer to the dendrimer periphery, and (iii) the different intermolecular hydrogen bond levels as a function of the pH and the structural details of the dendrimer.

Finally, the free energies of binding between the dendrimers and the NA fragment as estimated via the MM/PBSA approach confirm that high dendrimer generations of the examined topologies are required for efficient siRNA complexation. In particular, the values of $\Delta G_{bind}/N$ (i.e., the values of the binding free energy normalized by the

total number of charges on the dendrimer molecule at a given pH) highlight the substantial difference in affinity between nanocarriers of G4 and G5–G6, yielding the basis of a molecular rationale for the experimentally observed enhanced efficacy of these high G vectors in cell transfection experiments.[35,36,69] Furthermore, the analysis of the components of the binding free energies also reveals that two molecular design parameters play a major role in favoring nanovector/cargo interactions: (i) a substantial number of intermolecular hydrogen bonds between the dendrimer and the siRNA, which correlates with the enthalpy of the binding process, and (ii) the dendrimer flexibility associated mainly with the surface area, as expressed by the smaller entropy penalties paid by the more flexible dendrimers in enwrapping the siRNA molecule. As discussed above, one of the limiting step in the transfection efficiency of these dendrimer/siRNA based systems (and likely of all other nanovector-based delivery systems) is the endosomal escape. The escape from endosomes likely occurs via an activated fusion process of the oppositely charged endosome membrane and the dendrimer/siRNA complex. The activation energy of this process is proportional to the bending rigidity of the complex. Bending or deformation of the complex, as required by fusion, obviously results in an energy cost proportional to the overall complex rigidity. Thus, in principle, if the structural flexibility of the nanovector increases, the activation energy decreases, making fusion more likely; this finding is in line with the current experimental results for which the more flexible TEA-based dendrimers are more efficient in transfection than the intrinsically rigid NH3-core PAMAMs.

Combining the results from all the different analysis tools we have employed, it appears that for the PAMAM family dendrimers examined and at an experimentally realizable ionic strength, the main attributes related to an increased binding affinity between the two components in a qualitative sense are (i) the size of the dendrimer (the larger the generation the higher the binding affinity), (ii) the number of surface hydrogen-bonding-capable sites per dendrimer at pH conditions close to physiological levels (the larger the number the more efficient the binding), and (iii) the degree of structural flexibility of the dendritic structure (the higher the degree of flexibility the more favorable the binding due to the ability of the dendrimer to adapt its conformation appropriately in order to enwrap the siRNA strands).

Based on the above findings we believe that the present work offers new insight regarding the mechanisms involved in the dendrimer/siRNA complexation, contributing thus toward a better understanding of the function of PAMAM-like dendrimers as potential gene delivery systems.

Acknowledgements: K. K. would like to express his gratitude to the personnel of the Molecular Simulations Engineering (MOSE) Laboratory for the warm hospitality and the fruitful collaboration during his stay at the DI3 in Trieste. Part of this work was carried out under the HPC-Europa 2 project (CINECA Supercomputing Center, Bologna, Italy), funded by the European Commission — DG Research in the 7th Framework Program (Grant agreement no 228398). The present work was also performed in the framework of the European Science Foundation COST TD0802 action "Dendrimers in Biomedical Applications".

This paper was amended because of the replacement of Figures 4 and 5.

Received: July 13, 2011; Published online: December 6, 2011; DOI: 10.1002/mabi.201100276

Keywords: complexation; dendrimers; molecular dynamics; short interfering RNA (siRNA)

[1] I. J. Majoros, B. B. Ward, K. H. Lee, S. K. Choi, B. Huang, A. Myc, J. R. Baker, *Prog. Mol. Biol. Trans. Sci.* **2010**, *95*, 193.
[2] M. D. Brown, A. G. Schatzlein, L. F. Uchegbu, *Int. J. Pharm.* **2001**, *229*, 1.
[3] H. Mok, T. G. Park, *Macromol. Biosci.* **2009**, *9*, 731.
[4] E. Marshall, *Science* **2000**, *288*, 951.
[5] T. Dutta, N. K. Jain, N. A. J. Mcmillan, H. S. Parekh, *Nanomedicine-UK* **2010**, *6*, 25.
[6] C. Dufes, I. F. Uchegbu, A. G. Schatzlein, *Adv. Drug Delivery Rev.* **2005**, *57*, 2177.
[7] J. D. Eichman, A. U. Bielinska, J. F. Kukowska-Latallo, J. R. Baker, *Pharm. Sci. Technol. Today* **2000**, *3*, 232.
[8] S. H. Bai, C. Thomas, A. Rawat, F. Ahsan, *Crit. Rev. Ther. Drug Carrier Syst.* **2006**, *23*, 437.
[9] W. D. Jang, K. Kataoka, *J. Drug Delivery Sci. Technol.* **2005**, *15*, 19.
[10] D. G. Shcharbin, B. Klajnert, M. Bryszewska, *Biochemistry* **2009**, *74*, 1070.
[11] M. Krämer, J.-F. Stumbé, G. Grimm, B. Kaufmann, U. Krüger, M. Weber, R. Haag, *Chembiochem* **2004**, *5*, 1081.
[12] Y.-N. Xue, M. Liu, L. Peng, S.-W. Huang, R.-X. Zhuo, *Macromol. Biosci.* **2010**, *10*, 404.
[13] G. M. Pavan, P. Posocco, A. Tagliabue, M. Maly, A. Malek, A. Danani, E. Ragg, C. V. Catapano, S. Pricl, *Chem. Eur. J.* **2010**, *16*, 7781.
[14] V. Vasumathi, P. K. Maiti, *Macromolecules* **2010**, *43*, 8264.
[15] G. M. Pavan, A. Danani, S. Pricl, D. K. Smith, *J. Am. Chem. Soc.* **2009**, *131*, 9686.
[16] P. K. Maiti, B. Bagchi, *Nano Lett.* **2006**, *6*, 2478.
[17] S. P. Jones, G. M. Pavan, A. Danani, S. Pricl, D. K. Smith, *Chem. Eur. J.* **2010**, *16*, 4519.
[18] S. Pricl, P. Posocco, G. M. Pavan, M. Fermeglia, G. Scocchi, A. Danani, A. Malek, S. Napoli, C. V. Catapano, *Ejc Suppl.* **2008**, *6*, 173.
[19] G. M. Pavan, M. A. Mintzer, E. E. Simanek, O. M. Merkel, T. Kissel, A. Danani, *Biomacromolecules* **2010**, *11*, 721.
[20] D. Ouyang, H. Zhang, D.-P. Herten, H. S. Parekh, S. C. Smith, *J. Phys. Chem. B* **2010**, *114*, 9220.
[21] D. Ouyang, H. Zhang, H. S. Parekh, S. C. Smith, *J. Phys. Chem. B* **2010**, *114*, 9231.

[22] W. D. Tian, Y. Q. Na, *Macromolecules* **2010**, *43*, 1575.
[23] J. S. Klos, J. U. Sommer, *J. Chem. Phys.* **2011**, *134*, 204902.
[24] R. I. Gilmore, S. P. Fox, A. J. Hollins, S. Akhtar, *Curr. Drug Delivery* **2006**, *3*, 147.
[25] S. M. Elbashir, J. Harborth, W. Lendeckel, A. Yalcin, K. Weber, T. Tuschl, *Nature* **2001**, *411*, 494.
[26] X. X. Liu, P. Rocchi, F. Q. Qu, S. Q. Zheng, Z. C. Liang, M. Gleave, J. Iovanna, L. Peng, *ChemMedChem* **2009**, *4*, 1302.
[27] J. Zhou, J. Wu, N. Hafdi, J. Behr, P. Erbacher, L. Peng, *Chem. Commun. (Camb)* **2006**, 2362.
[28] L. Kumar, A. Clarke, *Adv. Drug Delivery Rev.* **2007**, *59*, 87.
[29] D. Gary, N. Puri, Y. Won, *J. Controlled Release* **2007**, *121*, 64.
[30] M. L. Patil, M. Zhang, S. Betigeri, O. Taratula, H. He, T. Minko, *Bioconjugate Chem.* **2008**, *19*, 1396.
[31] H. Kang, R. Delong, M. Fisher, R. Juliano, *Pharm. Res.* **2005**, *22*, 2099.
[32] H. Baigude, T. M. Rana, *ChemBioChem* **2009**, *10*, 2449.
[33] L. J. F. Kukowska, A. U. Bielinska, J. Johnson, R. Spindlerdagger, D. A. Tomalia, J. R. J. Baker, *Proc. Natl. Acad. Sci.* **1996**, *93*, 4897.
[34] U. Boas, S. H. M. Söntjens, K. J. Jensen, J. B. Christensen, E. W. Meijer, *ChemBioChem* **2002**, *3*, 433.
[35] X. Shen, J. Zhou, X. Liu, J. Wu, F. Qu, Z. Zhang, D. Pang, G. Quelever, C. Zhang, L. Peng, *Org. Biomol. Chem.* **2007**, *5*, 3674.
[36] C.-J. Su, H.-L. Chen, M.-C. Wei, S.-F. Peng, H.-W. Sung, V. A. Ivanov, *Biomacromolecules* **2009**, *10*, 773.
[37] A. U. Bielinska, C. Chen, J. Johnson, J. J. R. Baker, *Bioconjugate Chem.* **1999**, *10*, 843.
[38] J. S. Kłos, J. U. Sommer, *Macromolecules* **2010**, *43*, 10659.
[39] J. S. Kłos, J. U. Sommer, *Macromolecules* **2010**, *43*, 4418.
[40] S. V. Lyulin, I. Vattulainen, A. A. Gurtovenko, *Macromolecules* **2008**, *41*, 4961.
[41] G. M. Pavan, L. Albertazzi, A. Danani, *J. Phys. Chem. B* **2010**, *114*, 2667.
[42] J. Y. Wu, J. H. Zhou, F. Q. Qu, P. H. Bao, Y. Zhang, L. Peng, *Chem. Commun.* **2005**, 313.
[43] A. U. Bielinska, J. F. Kukowska-Latallo, J. J. Baker, *Biochim. Biophys. Acta* **1997**, *1353*, 180.
[44] J. Haensler, F. C. Szoka, *Bioconjugate Chem.* **1993**, *4*, 372.
[45] M. Serresi, R. Bizzarri, F. Cardarelli, F. Beltram, *Anal. Bioanal. Chem.* **2009**, *393*, 1123.
[46] E. Ragg, personal communication, 2011.
[47] M. Fermeglia, M. Ferrone, S. Pricl, *Bioorg. Med. Chem.* **2002**, *10*, 2471.
[48] L. Metullio, M. Ferrone, A. Coslanich, S. Fuchs, M. Fermeglia, M. Paneni, S. Pricl, *Biomacromolecules* **2004**, *5*, 1371.
[49] S. Pricl, M. Fermeglia, M. Ferrone, A. Asquini, *Carbon* **2003**, *41*, 2269.
[50] P. Posocco, M. Ferrone, M. Fermeglia, S. Pricl, *Macromolecules* **2007**, *40*, 2257.
[51] A. D. Mackerell, N. Banavali, N. Foloppe, *Biopolymers* **2000**, *56*, 257.
[52] N. Foloppe, A. D. Mackerell, Jr., *J. Comput. Chem.* **2000**, *21*, 86.
[53] E. Giudice, R. Lavery, *Acc. Chem. Res.* **2002**, *35*, 350.
[54] U. D. Priyakumar, A. D. J. Mackerell, *J. Chem. Theory Comput.* **2006**, *2*, 187.
[55] C. V. Kelly, P. R. Leroueil, E. K. Nett, J. M. Wereszczynski, J. R. Baker, B. G. Orr, M. M. B. Holl, I. Andricioaei, *J. Phys. Chem. B* **2008**, *112*, 9337.
[56] C. V. Kelly, P. R. Leroueil, B. G. Orr, M. M. Banaszak Holl, I. Andricioaei, *J. Phys. Chem. B* **2008**, *112*, 9346.
[57] A. Pedretti, L. Villa, G. Vistoli, *J. Comput. -Aided Mol. Des.* **2004**, *18*, 167.
[58] W. L. Jorgensen, J. Chandrasekhar, J. D. Madura, R. W. Impey, M. Klein, *J. Chem. Phys.* **1983**, *79*, 926.
[59] S. W. Poxon, P. M. Mitchell, E. Liang, J. A. Hughes, *Drug Delivery* **1996**, *3*, 255.
[60] W. Humphrey, A. Dalke, K. Schulten, *J. Mol. Graphics* **1996**, *14*, 33.
[61] S. E. Feller, Y. Zhang, R. W. Pastor, B. R. Brooks, *J. Chem. Phys.* **1995**, *103*, 4613.
[62] T. Darden, L. Perera, L. Li, L. Pedersen, *Structure* **1999**, *7*, R55.
[63] P. Posocco, S. Pricl, S. Jones, A. Barnard, D. K. Smith, *Chem. Sci.* **2010**, *1*, 393.
[64] J. Srinivasan, T. E. Cheatham, P. Cieplak, P. A. Kollman, D. A. Case, *J. Am. Chem. Soc.* **1998**, *120*, 9401.
[65] K. Karatasos, D. B. Adolf, G. R. Davies, *J. Chem. Phys.* **2001**, *115*, 5310.
[66] S. Huissmann, A. Wynveen, C. N. Likos, R. Blaak, *J. Phys.: Condens. Matter* **2010**, *22*, 232101.
[67] S. Huissmann, C. N. Likos, R. Blaak, *J. Mater. Chem.* **2010**, *20*, 10486.
[68] I. Tanis, K. Karatasos, *Phys. Chem. Chem. Phys.* **2009**, *11*, 10017.
[69] X. Liu, J. Wu, M. Yammine, J. Zhou, P. Posocco, S. Viel, C. Liu, F. Ziarrelli, M. Fermeglia, S. Pricl, G. Victorero, C. Nguyen, P. Erbacher, J.-P. Behr, L. Peng, unpublished.
[70] O. Boussif, F. Lezoualc'h, M. A. Zanta, M. D. Mergny, D. Scherman, B. Demeneix, J.-P. Behr, *Proc. Natl. Acad. Sci. U. S. A.* **1995**, *92*, 7297.
[71] L. Porcar, K. Hong, P. D. Butler, K. W. Herwig, G. S. Smith, Y. Liu, W.-R. Chen, *J. Phys. Chem. B* **2010**, *114*, 1751.
[72] Y. Liu, C. Y. Chen, H. L. Chen, K. Hong, C. Y. Shew, X. Li, L. Liu, Y. B. Melnichenko, G. S. Smith, K. W. Herwig, L. Porcar, W. R. Chen, *J. Phys. Chem. Lett.* **2010**, *1*, 2020.
[73] G. Nisato, R. Ivkov, E. J. Amis, *Macromolecules* **2000**, *33*, 4172.
[74] K. Fant, E. K. Esbjorner, P. Lincoln, B. Norden, *Biochemistry* **2008**, *47*, 1732.
[75] A. Shakhbazau, I. Isayenka, N. Kartel, N. Goncharova, I. Seviaryn, S. Kosmacheva, M. Potapnev, D. Shcharbin, M. Bryszewska, *Int. J. Pharm.* **2010**, *383*, 228.
[76] M. H. Kleinman, J. H. Flory, D. A. Tomalia, N. J. Turro, *J. Phys. Chem. B* **2000**, *104*, 11472.
[77] M. Santo, M. A. Fox, *J. Phys. Org. Chem.* **1999**, *12*, 293.
[78] S. Zimmerman, L. Lawless, *Top Curr. Chem.* **2001**, *217*, 95.
[79] M. Liu, J. M. J. Frechet, *Pharm. Sci. Technol. Today* **1999**, *2*, 393.
[80] J. F. G. A. Jansen, E. M. M. De Brabander-Van Den Berg, E. W. Meijer, *Science* **1994**, *266*, 1226.
[81] I. Tanis, K. Karatasos, *J. Phys. Chem. B* **2009**, *113*, 10984.
[82] I. Tanis, K. Karatasos, *Macromolecules* **2009**, *42*, 9581.
[83] M. Mammen, S. K. Choi, G. M. Whitesides, *Angew. Chem., Int. Ed. Engl.* **1998**, *37*, 2754.
[84] A. Bielinska, J. F. Kukowska-Lataloo, J. Johnson, D. A. Tomalia, J. Baker, *Nucleic Acids Res.* **1996**, *24*, 2176.
[85] E. Chiessi, F. Cavalieri, G. Paradossi, *J. Phys. Chem. B* **2007**, *111*, 2820.
[86] G. A. Jeffrey, W. Saenger, *Hydrogen Bonding In Biological Structures*, Springer-Verlag, Berlin **1991**.
[87] H. Lee, J. R. Baker, R. G. Larson, *J. Phys. Chem. B* **2006**, *110*, 4014.
[88] J. C. Speakman, *The Hydrogen Bond And Other Intermolecular Forces*, The Chemical Society, London **1975**.
[89] L. Porcar, Y. Liu, R. Verduzco, K. L. Hong, P. D. Butler, L. J. Magid, G. S. Smith, W. R. Chen, *J. Phys. Chem. B* **2008**, *112*, 14772.